2018-01-1255

Efficiency and Emissions Characteristics of an HCCI Engine Fueled by Primary Reference Fuels

Author, co-author (Do NOT enter this information. It will be pulled from participant tab in MyTechZone)

Affiliation (Do NOT enter this information. It will be pulled from participant tab in MyTechZone)

Abstract

This paper investigates the effects of various primary reference fuel (PRF) blends, compression ratios, and intake temperatures on the thermodynamics and performance of homogeneous charge compression ignition (HCCI) combustion in a CFR engine. Combustion phasing was kept constant at a CA50 phasing of 5° aTDC and the equivalence ratio was kept constant at 0.3. Meanwhile, the compression ratio varied from 8:1 to 15:1 as the PRF blends ranged from pure n-heptane to nearly pure isooctane. The intake temperature was used to match CA50 phasing. In addition to the experimental results, a GT-Power model was constructed to simulate the experimental engine and the model was validated against the experimental data. The GT-Power model and simulation results were used to help analyze the energy flows and thermodynamic conditions tested in the experiment.

The results indicate that an increase of compression ratio causes higher thermal efficiency and fuel conversion efficiency; however, at the same compression ratio, an increase in PRF number results in lower efficiency due to the required increase in intake temperature and the associated decrease in charge density. While the efficiency does increase with compression ratio, the results show that the effect of increased expansion work is partially offset by higher heat transfer losses and lower ratios of specific heats at higher compression ratios. The results indicate that the maximum pressure rise rate (MPRR) in HCCI significantly increases with compression ratio. Combustion efficiency shows a strong trend with peak temperature regardless of the PRF number or compression ratio, indicating that the CO to CO_2 conversion is independent of the parent fuel chemistry in the case of the primary reference fuels; whereas the unburned hydrocarbon emissions showed the opposite trend, depending mostly on the parent fuel's autoignition tendency.

Introduction

Homogeneous charge compression ignition (HCCI) combustion was first conceptualized in late 1970s and early 1980s [1-3]. As a combination of the favorable attributes of homogeneous spark ignition (SI) combustion and conventional diesel compression ignition (CI) combustion, HCCI is a combustion mode with high efficiency and low emissions [4-8]. Previous research work has shown that increased thermal efficiency can be achieved in HCCI compared with traditional SI combustion, and the efficiency can be as high as direct injection CI combustion. This is due to lower equivalence ratios, higher compression ratios, and the elimination of the throttle. Meanwhile, the decreased in-cylinder temperature reduces heat transfer losses and nitrogen oxides emissions, while soot emissions are avoided by premixing the fuel and air. Furthermore, a wide range of fuels can be applied to an engine operating on HCCI combustion, including gasoline, diesel, sustainable biofuels, and electrofuels, which presents a future solution for transportation applications that is simultaneously clean and efficient and uses a sustainably produced fuel that could be carbon-neutral [9-14].

Based on the above-mentioned benefits of HCCI combustion, it is not surprising that HCCI has been a focal point of major research efforts over the past 30 years [15-28]. In HCCI combustion, ignition is controlled by the chemical kinetics of the fuel, as well as the properties of the mixture and the time-temperature histories of various regions, which means that ignition is not as easily controlled as SI or conventional diesel combustion [29-31]. Another disadvantage of HCCI is the large quantities of unburned hydrocarbons and carbon monoxide emissions caused by the low burned gas temperatures. Finally, the combustion duration in HCCI is significantly shorter than SI and diesel combustion, which can be an advantage, but also results in high pressure rise rates at relatively low loads, which limits the maximum engine load in HCCI [32, 33].

Due to these disadvantages, the combustion process needs to be better understood in order to regulate the ignition, thermal stratification, and heat release rate to gain better control, higher efficiency, and lower emissions over a range of loads that satisfy practical requirements [34, 35]. To this end, research efforts have investigated the effects of various parameters on HCCI combustion [36, 37]. Based on these fundamental and experimental studies, several engine control strategies have been established to help adjust the mixture reactivity and time-temperature histories. Methods such as exhaust gas recirculation (EGR), variable valve timing (VVT), variable compression ratio (VCR), and varying the fuel's autoignition properties are widely discussed in previous papers and are proved viable solutions for control over ignition in HCCI [38-41].

Among all of these techniques, intake temperature is most easily adjusted and controlled in a laboratory setting. Additionally, compression ratio is known to be an important parameter that dictates engine performance. These two operating parameters, intake temperature and compression ratio, are highly coupled in HCCI combustion, and have therefore been investigated together. Christensen et al explained that almost all liquid fuels could be autoignited by changing the compression ratio [38, 42]. Haraldsson et.

al applied HCCI in a multi-cylinder engine to develop a relationship between compression ratio and intake temperature, and realized that higher compression ratios can be used in place of higher intake temperatures to get better thermal efficiency and lower NOx emissions [43]. Further experiments on the effects of fuel properties and compression ratio on efficiency were provided by Szybist et. al [44], who showed that thermal efficiency increased with compression ratio while the intake air was used to maintain CA50 constant. However, with increasing compression ratio, especially to very high values, the heat transfer losses can increase as well, which can reduce the thermal efficiency. This motivates the need for an in-depth investigation of compression ratio, intake temperature, and fuel properties on the efficiency of HCCI and the trade-offs that exist. The abovementioned studies were focused on several mixtures with different components and mixing rates. This paper uses a CFR engine with a wide range of compression ratios and PRF fuel blends to help better understand the relationship between the compression ratio, intake temperature, and fuel blend in HCCI combustion.

The fuel's autoignition tendency is a key factor that highly influences the ignition timing and heat release process in HCCI. Iso-octane and n-heptane are the two primary reference fuels (PRFs) used to achieve variable autoignition properties that span the range of autoignition tendencies that are most relevant to commercial gasoline and diesel fuels. However, fuels with the same research octane number but different compositions can have different combustion characteristics [45]. Using PRF mixtures in combustion testing can therefore provide meaningful information about the ignition timings and burn rates relevant to commercial multicomponent fuels [46-49].

In this paper, a very wide range of primary reference fuels was tested in a Cooperative Fuels Research (CFR) engine operating in HCCI mode at various compression ratios. This data helped to develop a deeper understanding of the effects of compression ratio and intake temperature on the thermodynamics and emissions of HCCI combustion. Experiments were performed using 28 different PRF blends varying from PRF0 to PRF96. The intake temperature and compression ratio were adjusted to keep the CA50 combustion phasing fixed at 5° aTDC, while the equivalence ratio was kept constant at 0.3. The effect of PRF number on cylinder pressure, mean cylinder temperature, instantaneous and cumulative heat loss, the ratio of specific heats, the heat release rate, the indicated mean effect pressure (IMEP), and the indicated efficiency are discussed below.

Methodology

Experimental Setup and Procedure

The experiment was conducted on a single-cylinder, port fuel injected, Waukesha CFR engine. Figure 1 illustrates the experimental setup and Table 1 shows the specifications of the engine. The engine was connected to a General Electric DC dynamometer. The air flow rate was controlled using a mass flow controller with accuracy of ±1%, and the fuel flow rate was measured by a Micro Motion Coriolis fuel flow meter (CMFS007M) with accuracy of ±0.25%. The above data were used to calculate the equivalence ratio and compared with the air-fuel ratio calculated from the emissions, which were measured with a Horiba MEXA-7100DEGR motor exhaust gas analyzer. The intake air was heated by an inline resistive heater and was PID-controlled to provide the desired intake temperature measured at the intake port. The PRF blends were premixed before being added to the fuel tank. The instantaneous cylinder pressure was acquired and triggered by the crankshaft encoder at a frequency of 1800 pulses per revolution (0.2 crank angle degree resolution). A Kistler 7061B pressure transducer was used to measure the cylinder pressure. The signal was then converted to voltage using a Kistler model 5010B amplifier with accuracy of ±0.5%. Two hundred consecutive cycles were recorded for each operating point. The pressure and temperature of the oil, coolant, and intake air were measured by pressure transducers and thermocouples, respectively. The oil and coolant were preheated to their set points and maintained constant by Omega PID controllers. EGR was not used in this experiment. The intake pressure was fixed

Table 1. Specifications of the CFR engine

Engine configuration	Single cylinder
Bore [mm]	82.5
Stroke [mm]	114.3
Displacement [L]	0.612
Compression ratio	6:1 – 18:1
Intake pressure [kPa]	98
Coolant temperature [K]	363
Oil temperature [K]	334
Number of valves	2
IVO [°ATDC]	-350
IVC [°ATDC]	-146
EVO [°ATDC]	140
EVC [°ATDC]	-345
Connecting rod length [mm]	254
Engine speed [RPM]	1200

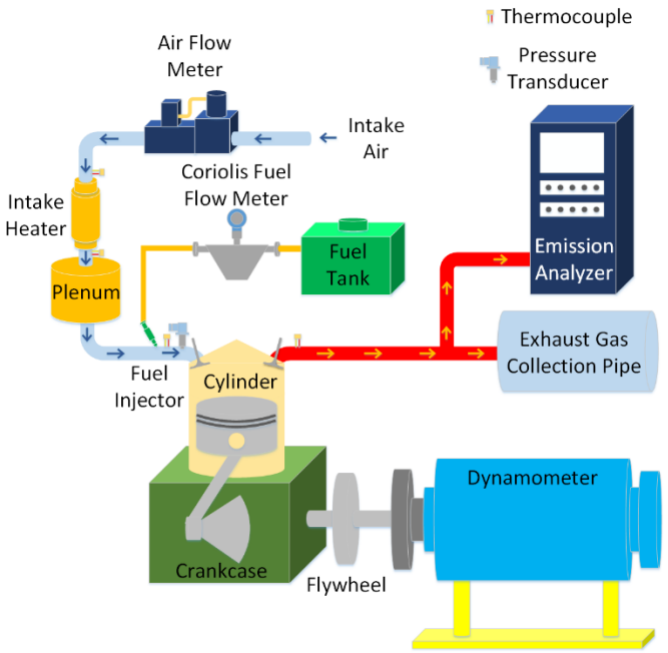

Figure 1. Schematic of the experimental setup

All the signals were recorded with National Instruments hardware and a custom, in-house LabVIEW data acquisition code. The code allows for real-time monitoring of load, efficiency, emissions, and heat release characteristics including CA50 such that the equivalence ratio

and CA50 combustion phasing could be matched during the experiment to the target values of 0.3 and 5° aTDC, respectively.

Parameter Calculation Methodology

The gross heat release rate was calculated by the following equation:

$$\frac{dQ}{d\theta} = \frac{\gamma}{\gamma-1} \times \frac{pdV}{d\theta} + \frac{1}{\gamma-1} \times \frac{Vdp}{d\theta} + \frac{dQ_{loss}}{d\theta} \quad (1)$$

where $\frac{dQ}{d\theta}$ is the gross heat release rate, θ is the crank angle degree, γ is the ratio of specific heats of the mixture calculated from the NASA polynomials at each time step using the current pressure, temperature, and mixture properties, p is the instantaneous cylinder pressure, V is the instantaneous cylinder volume, and $\frac{dQ_{loss}}{d\theta}$ is the heat loss to the walls.

The gross heat release rate was calculated by adding the heat loss to the cylinder walls to the net heat release rate. The mean cylinder temperature was calculated using the ideal gas law. The wall temperature was assumed to be 400 K. The heat loss is determined via the following equation:

$$Q_{loss} = hA(T - T_{wall}) \quad (2)$$

where h is the convective heat transfer coefficient, A is the total cylinder surface area, T is the in-cylinder mean temperature, and T_{wall} is the wall temperature.

The heat transfer coefficient was calculated using the Hohenberg heat transfer correlation [50]:

$$h = C_1 \times V^{-0.06} \times p^{0.8} \times T^{-0.4} \times (\overline{v_p} + C_2)^{0.8} \quad (3)$$

where $\overline{v_p}$ is the mean piston speed, C_1 is a constant defined as 130, and C_2 is a constant defined as 1.4.

Modeling Methodology

In addition to the experimental setup, a system-level model was constructed in GT-Power to further analyze the thermodynamic conditions and considerations related to the experimental data. Figure 2 shows the model as it appears in the modeling interface. GT-Power performs 1-D flow calculations in the pipes and a 0-D thermodynamic calculation in the cylinder. The 1-D flow model uses the Navier-Stokes equation, averaged across the cross-section of the pipe. The operating conditions supplied to the model were acquired from the experiment. The heat release rate was calculated using Equations (1) - (3) from the experimental cylinder pressure, and then specified to the corresponding model object as an input. The model was validated against the experimental pressure trace at every condition analyzed. A few example cases are shown in Figure 3. This figure demonstrates the validity of the model based on the agreement between the measured and simulation cylinder pressure under low, medium, and high PRF numbers. In the following sections, a large amount of results will be discussed and compared. Among these data, the intake temperature and emissions are directly measured from the experiment, the heat release rate is calculated from the experimental data and used as an input to the GT-Power model, and the remaining results are from the GT-Power simulations.

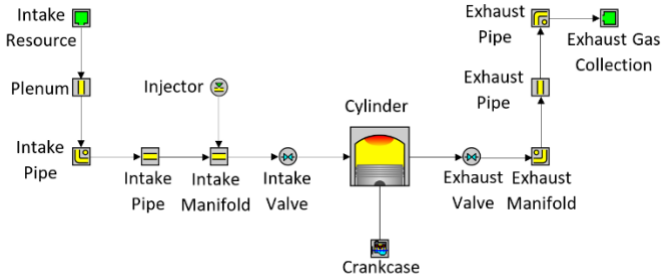

Figure 2. Schematic of the simulation model

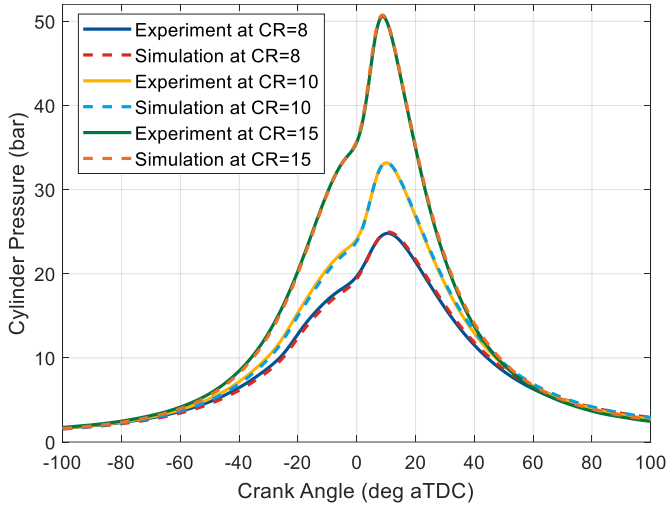

Figure 3. Comparison between experimental and simulated cylinder pressure at three different compression ratios and PRF numbers

Results and Discussion

In this paper, an extended discussion of the thermodynamics that result from a combination of PRF number, compression ratio (CR), and intake temperature is provided. Figure 4 shows the intake temperature that was required to achieve HCCI combustion with an equivalence ratio of 0.3 and a CA50 of 5° aTDC for each PRF blend and compression ratio. Due to experimental limitations, the range of possible intake temperatures is approximately 310 K to 400 K. Additionally, operational limits on the maximum pressure rise rate and the coefficient of variation (COV) of net indicated mean effective pressure (IMEPn) were defined as 5 bar/degree and 5%, respectively. All of the cases shown in Figure 4 are within these limits.

Figure 4 clearly shows that as the PRF number increases, the intake temperature also needs to increase to keep CA50 constant at a given compression ratio. The range of possible intake temperatures with this experimental setup is 310 K to 400 K. The intake temperature cannot exceed 400 K due to the temperature limits of some of the materials and components in the intake system, and the minimum intake temperature is 310 K. Alternatively, increasing the compression ratio can also be used to autoignite higher PRF number fuels by increasing the temperature around TDC for a given intake temperature. At low compression ratios, the engine operation was generally more robust (i.e. lower maximum pressure rise rate, lower COV of IMEP, and generally lower sensitivity to changes in intake temperature and compression ratio), which led to the collection of more data at the lower compression ratios and lower PRF numbers. For example, at CR

= 9, nine different cases are acquired with the maximum difference in PRF number being 26 points with the difference in intake temperature for the highest and lowest PRF numbers being 76.6 K. For compression ratios in the middle of the range, the fewest cases were collected since the engine was generally less stable and required larger changes in intake temperature. At CR of 11, only two cases could be collected in the range of possible intake temperatures, which were PRF60 and PRF63 with a temperature difference of 25 K. This was attributed to the transition from two-stage heat release to single-stage heat release in the mid-range of the PRF number scale, but will be investigated further in future work. At higher compression ratios of 14 and 15, the engine operation was slightly more predictable and the temperature gap between PRF number increments of 3 decreased, which allowed three cases to be collected for each compression ratio (e.g. the difference between maximum and minimum cases is 33K or less which is smaller than the same value at a compression ratio of 13).

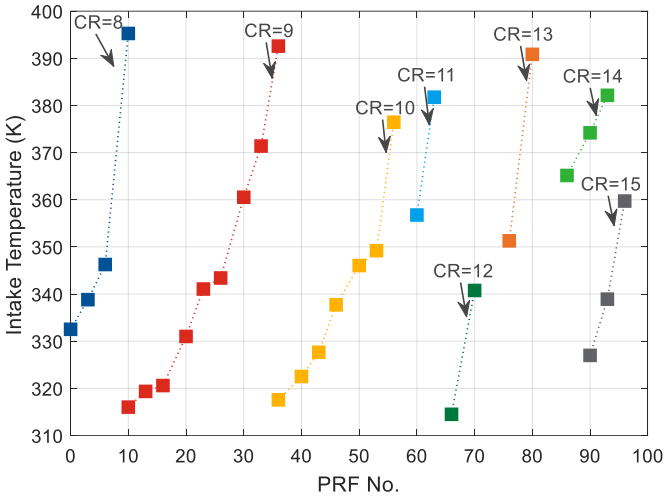

Figure 4. Intake temperature requirements to achieve HCCI combustion at an equivalence ratio of 0.3 and a CA50 combustion phasing of 5° aTDC for varying PRF number and compression ratio

Cylinder Pressure and Pressure Rise Rate

Different conditions are selected to compare various PRF blends and compression ratios at a constant intake temperature of approximately 340 K. These cases are shown in Table 2. In the following sections, these selected cases are used to elaborate on both the combustion characteristics and thermodynamic considerations with different compression ratio and PRF number. The selected pressure traces are illustrated in Figure 5. With the increase in PRF number, compression ratio also increases which causes the peak pressure to increase from 25.0 bar to 52.1 bar. The position of peak pressure slightly advances from 10.8° aTDC to 8.8° aTDC as the compression ratio and PRF number increase (even though CA50 is constant).

Since the cylinder pressures are fairly self-similar, the variation in peak pressure can be used to represent the pressure throughout the cycle. Figure 6 shows a plot of the peak pressure for all of the operating conditions shown in Figure 4. As can be seen, the peak pressure increases significantly with increasing compression ratio and PRF number. When the compression ratio is constant, the peak pressure slightly decreases with increasing PRF number, which could possibly be due to the higher intake temperatures decreasing the density of the incoming air-fuel mixture. Since the equivalence ratio was constant for all cases, lower incoming densities also translated to slightly lower loads, which is due to the effects of intake temperature on density and load. Comparison between the specific cases at constant intake temperature (i.e. the cases in Table 2) is required and will be shown through the remainder of this paper. In Figure 6, at the lower compression ratios, the trend line of peak pressure versus PRF number is almost flat with a reduction of 1.4 bar in peak pressure from PRF3 to PRF10 at CR = 8. However, at the higher compression ratios, the peak pressure decreases more sharply as the intake temperature reduces the density of the incoming air. At CR = 15, the difference in peak pressure is 5.8 bar between PRF 90 and PRF96. This shows that the density variations due to intake temperature changes are amplified at higher compression ratios.

Table 2. Parameters of selected cases with approximately constant intake temperature

Case No.	PRF No.	CR	Tintake (K)
1	3	8	339
2	23	9	341
3	46	10	338
4	70	12	341
5	93	15	339

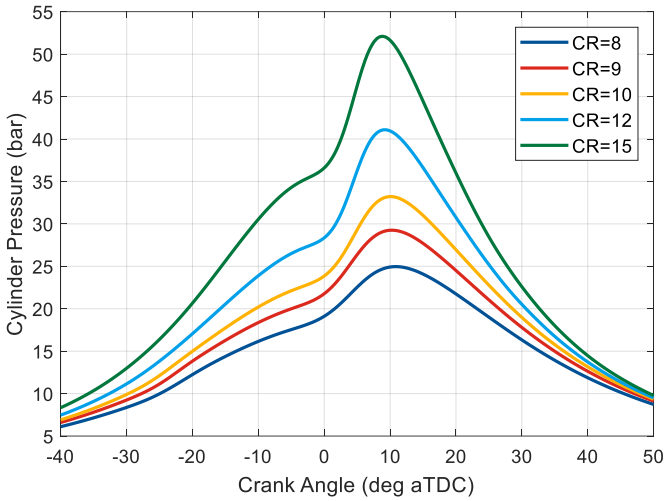

Figure 5. Cylinder pressure for the selected cases in Table 2

Figure 7 shows the MPRR for all cases. A similar trend occurs for the MPRR in Figure 7 as the peak pressure in Figure 6. As the compression ratio and PRF number increase, the MPRR strongly increases by a factor of 4 from the lowest PRF number cases to the highest. At the highest compression ratio cases, there is a strong negative slope of MPRR with increasing PRF number, possibly due to the decreasing density and load with increasing intake temperature. These results show that the pressure rise rates in HCCI combustion increase with compression ratio. Therefore, lower compression ratios could potentially allow an increase in the upper load limit, if the maximum pressure rise rate defines the upper load limit. The maximum value in Figure 7 is 3.7 bar/CA at PRF90.

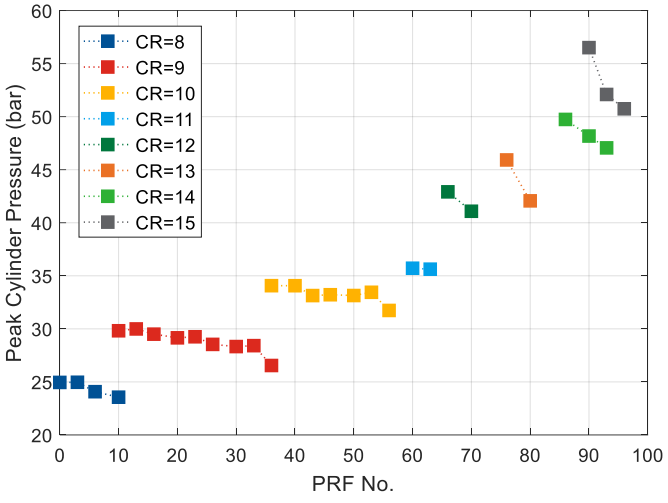

Figure 6. Peak pressure at different compression ratios versus PRF number for all of the data collected

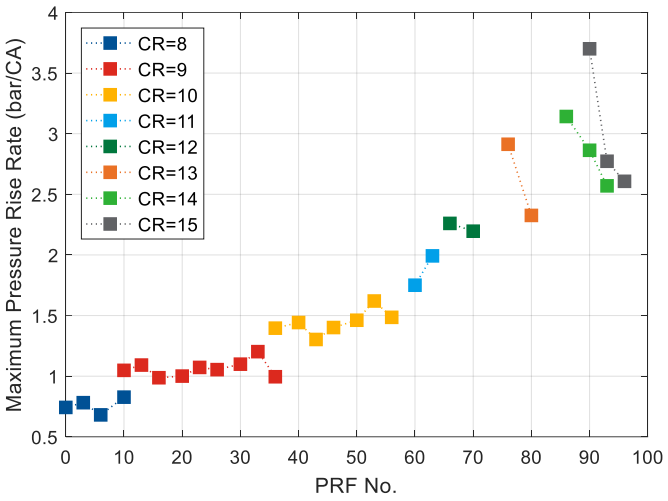

Figure 7. Maximum pressure rise rate at different compression ratios versus PRF number for all of the data collected

Bulk Gas Temperature

Figure 8 shows the in-cylinder bulk gas temperature (i.e. the average or mean cylinder temperature), which is calculated from the ideal gas law. The gas temperature is not able to be as simply characterized by its peak value like the cylinder pressure since the temperatures are not self-similar. Instead, the temperatures cross over each other during the expansion stroke. Before approximately 30° aTDC, the temperature increases with increasing compression ratio. Starting around 25° before TDC, the low temperature heat release (LTHR) can be seen in the lower compression ratio and lower PRF number cases. The LTHR causes the temperature to increase for the low compression ratio cases. The temperature then increases due to the high temperature heat release (HTHR) and reaches the peak value about 10° to 15° aTDC. The position of peak temperature advances slightly with increasing compression ratio. The latest peak temperature is at 15.4° aTDC with value 1368 K. The earliest peak temperature is as advanced as 11.2° aTDC with value 1510 K. The temperature then begins to decrease due to expansion; however, the higher compression ratio cases expand and reduce the temperature at a faster rate than the lower compression ratio cases. This causes the higher compression ratio cases to have a lower temperature throughout the majority of the expansion process. Meanwhile, the lower compression ratio cases have a higher temperature throughout the expansion process after around 35° aTDC, which will have implications on the heat transfer losses discussed later in this paper. It is important to note the differences in peak temperature are greater than 150 K from CR = 15 to CR = 8, despite the constant equivalence ratio and combustion phasing. At the equivalence ratio considered in this work, the NOx emissions were near-zero. However, when operating at equivalence ratios that result in peak temperatures closer to the NOx production threshold, these results indicate that a lower compression ratio might be beneficial for reducing the peak temperatures and reducing NOx emissions.

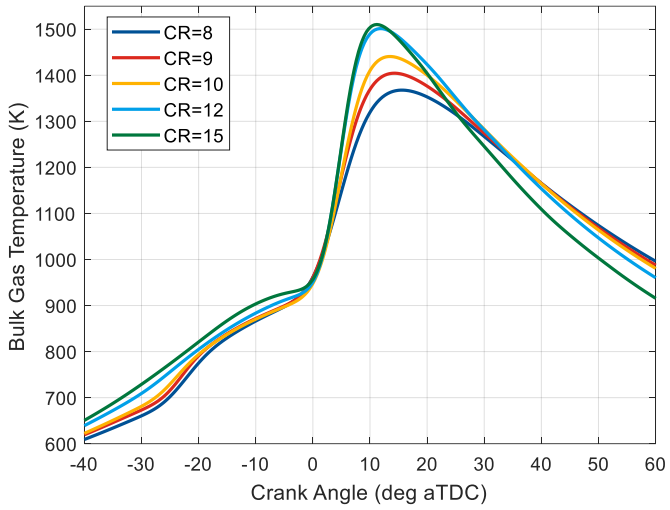

Figure 8. Bulk gas temperature for the selected cases in Table 2

Ratio of Specific Heats

In this paper, the ratio of specific heats is determined from the temperature, pressure, and composition of the mixture at each time step using the NASA polynomials. Figure 9 shows the ratio of specific heats for the selected cases in Table 2. In Figure 9, the ratio of specific heats decreases through the compression process due to the increasing mixture temperature. The effect of the LTHR on the bulk temperature can be seen in the ratio of specific heats for the lowest compression ratio cases (and therefore lowest PRF number cases), where the higher temperatures caused by the LTHR result in lower ratios of specific heats. All of the cases have very similar values around TDC. The highest compression ratio cases have the lowest ratios of specific heats during combustion due to the high temperatures. However, the ratio of specific heats for the high compression ratio cases is the highest after about 35° aTDC due to the expansion effects on the bulk temperature. These results show that the ratio of specific heats strongly depends on the in-cylinder temperature. The higher the in-cylinder temperature, the lower the ratio of specific heats.

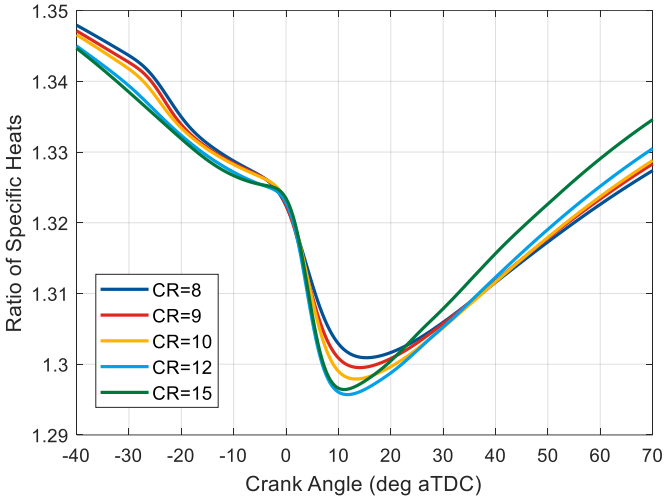

Figure 9. Ratio of specific heats for the selected compression ratio cases in Table 2

Figure 10 shows the minimum of ratio of specific heats for all cases. In the plot, the minimum specific heat ratio decreases when the compression ratio increases. Also, the ratio of specific heats decreases when the intake temperature increases. These two factors cause a general downward trend of the ratio of specific heats as the PRF number increases. The higher compression ratios will result in higher thermal efficiencies; however, these results show that that effect will be slightly counteracted by the lower ratios of specific heats.

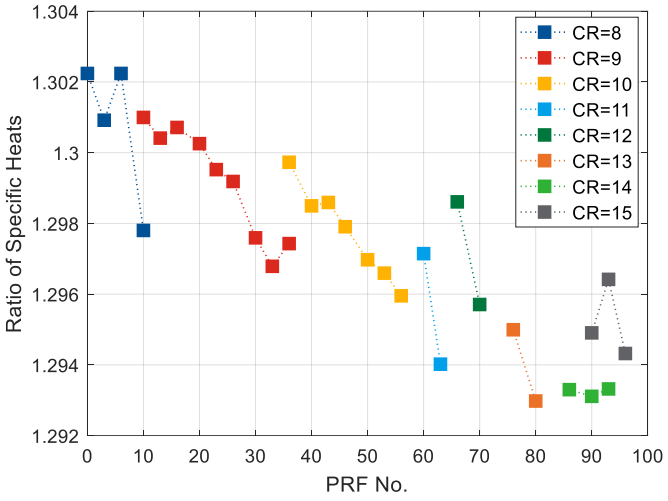

Figure 10. Minimum ratio of specific heats at different compression ratios versus PRF number for all of the data collected

Heat Release Rate

The gross heat release rate is calculated using the cylinder pressure, Equation (1), and the Hohenberg heat transfer correlation as discussed above. The resulting heat release rates are shown in Figure 11. Based on the results, combustion can be characterized by a two-stage heat release process, which includes LTHR and HTHR. It is worth noting that the LTHR peak is maximum at the lowest compression ratio and PRF number cases and minimum at the highest compression ratio and PRF number cases. LTHR in HCCI has been observed in the literature previously when using n-heptane or low PRF number mixtures as the fuel [44]. Combustion for the high PRF number fuels (above PRF73) can be classified as an approximately single-stage heat release process, where only minor LTHR happens before TDC. Recall that this LTHR had a significant impact on the temperature and ratio of specific heats as discussed above.

The peak LTHR decreases with increasing compression ratio because the PRF number increases; however, the crank angle timing of the peak LTHR also advances. The maximum HTHR shows the opposite trend, where the peak HTHR rises from 27 J/CA to 51 J/CA with increasing compression ratio. As the peak of the HTHR increases, the duration of the heat release process also decreases (since the area under the curves is approximately constant). This transition from two-stage to single-stage heat release and the shortening of the duration of the main HTHR helps to explain the increase in the maximum pressure rise rate in Figure 7. The peak HTHR timing is close to a constant value of approximately 5.8 aTDC. However, the single-stage versus two-stage heat release is not the only reason for the higher maximum pressure rise rates at higher PRF number. At PRF10, PRF36, PRF90, and PRF93, two different compression ratio cases exist (CR = 8 vs. CR = 9, CR = 9 vs. CR = 10, CR = 14 vs. CR = 15, and CR = 14 vs. CR = 15, respectively). From these comparisons, it can be seen that the pressure rise rate is always higher at the higher compression ratio, even when the fuel is constant. This result shows that higher compression ratios result in higher maximum pressure rise rates in HCCI. Therefore, lower compression ratios and/or two stage ignition fuels could be used to enable higher loads in HCCI.

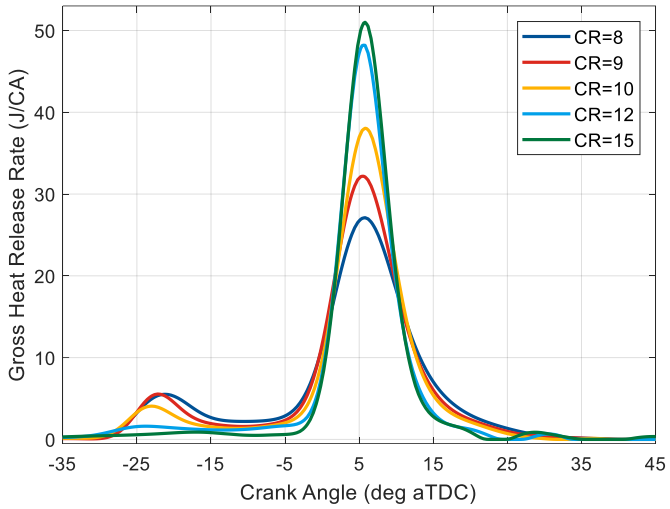

Figure 11. Gross heat release rate for the selected compression ratio cases in Table 2

Gross Indicated Mean Effective Pressure

The gross indicated mean effective pressure (IMEPg) is defined as the IMEP calculated over the compression and expansion strokes. The result is shown in Figure 12. For each individual compression ratio case, the IMEPg decreases while intake temperature increases, which means that under the same combustion phasing the engine load is strongly affected by intake temperature due to the density differences. Changing the PRF number or the compression ratio only has a small effect where the higher PRF numbers and higher compression ratios have slightly higher loads, which will be explained later in the discussion surrounding Figure 17.

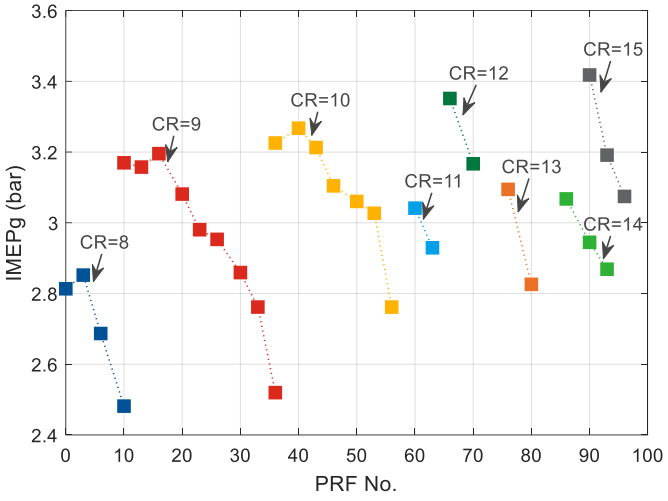

Figure 12. IMEPg at difference compression ratios versus PRF number for all of the data collected

Heat Loss and Heat Transfer Coefficient

As described in the Parameter Calculation Methodology section above, the heat transfer to the walls was estimated with the Hohenberg heat transfer correlation. Figure 13 and Figure 14 show the heat transfer coefficient of the selected cases in Table 2 and the peak values of the coefficient for all of the data collected, respectively. Figure 13 shows that the heat transfer coefficient increases with compression ratio. The heat transfer coefficient increases due to the compression process, then due to combustion, but expansion causes the heat transfer coefficient to decrease. The peak value of the heat transfer coefficient is able to capture the trend of the curves since the heat transfer coefficient is self-similar. Therefore, the peak values of the heat transfer coefficient for all of the data collected are illustrated in Figure 14. The data show a distinct conclusion that the maximum heat transfer coefficient increases with increasing compression ratio, and decreases slightly with increasing intake temperature. According to the Hohenberg correlation, the heat transfer coefficient is affected by the bulk gas temperature and the cylinder pressure. Recall from Figure 5 and Figure 6 that the cylinder pressure increases with compression ratio and decreases with intake temperature, which closely matches the trend in the heat transfer coefficient.

Figure 15 shows the instantaneous heat loss calculated using Equation (2). During the compression stroke, the heat loss rate increases with increasing compression ratio. This is due to the higher heat transfer coefficient along with the higher bulk gas temperatures, which causes a larger heat transfer rate for the higher compression ratio cases. Additionally, other researchers have shown that the higher pressure rise rates associated with higher compression ratio is another factor that can cause higher heat losses because the pressure oscillations break up the thermal boundary layer [44]. Although this effect is not captured in Equations (2) and (3) or Figure 15 and Figure 16, it is an important consideration for how the heat transfer losses change with compression ratio and pressure rise rates. Throughout combustion, the heat transfer rate is higher for the higher compression ratios due to the higher temperatures and heat transfer coefficient, despite the fact that the surface area of the higher compression ratio cases is slightly lower around TDC. During the expansion stroke at around 42° aTDC, there is a cross-over point beyond which the higher compression ratio cases have a lower heat transfer rate. This happens due to the trends in the bulk gas temperature discussed surrounding Figure 8. In short, the higher compression ratio cases expand the gases further than the lower compression ratio cases, which causes the temperatures during the expansion stroke for the higher compression ratio cases to decrease below that of the lower compression ratio cases. Since the heat loss is the result of multiplying the heat transfer coefficient, surface area, and the temperature difference, the lower in-cylinder temperatures can overpower the higher heat transfer coefficient for the higher compression ratio cases during the expansion stroke (after 42° aTDC). The cumulative heat loss over the closed portion of the cycle is shown in Figure 16. The cumulative heat loss increases with both compression ratio and intake temperature; however, the lower heat transfer rate during expansion for the higher compression ratio cases partially offsets the increase. As a result, the heat transfer losses are only 27% larger for the CR = 15 cases compared to the CR = 8 cases. In a similar fashion to the ratio of specific heats, these increasing heat transfer losses will attenuate the increase in efficiency with compression ratio, as discussed below.

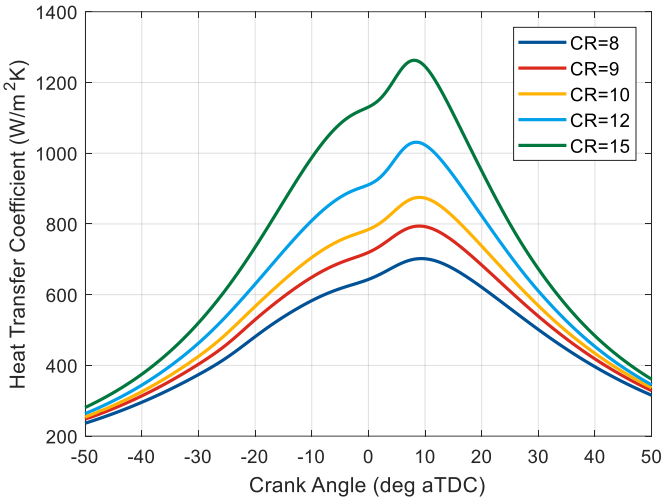

Figure 13. Heat transfer coefficient for the selected compression ratio cases in Table 2

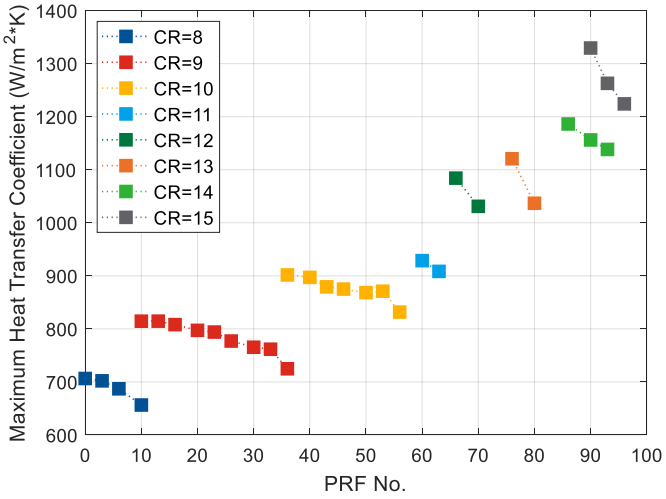

Figure 14. Maximum heat transfer coefficient at different compression ratios versus PRF number for all of the data collected

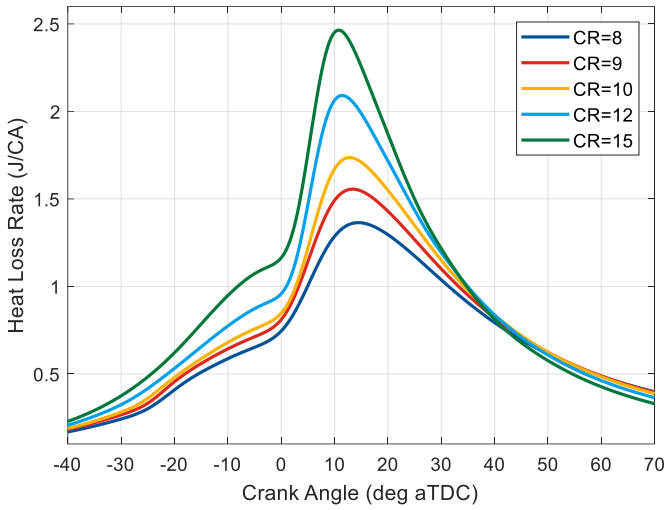

Figure 15. Instantaneous heat loss for the selected compression ratio cases in Table 2

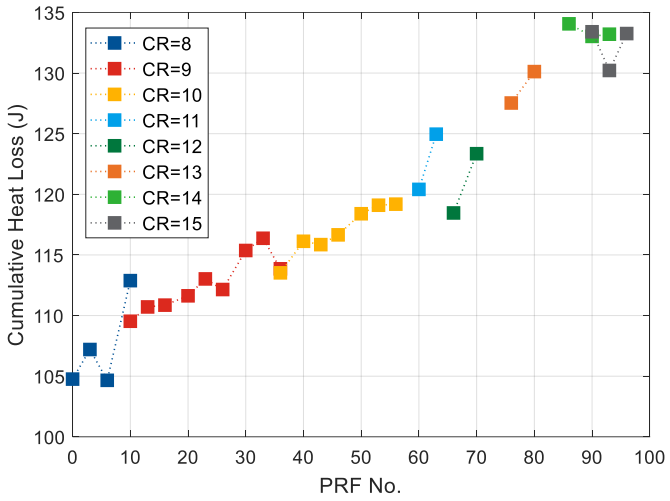

Figure 16. Cumulative heat loss at different compression ratios versus PRF number for all of the data collected

Thermal Efficiency and Fuel Conversion Efficiency

Figure 17 shows the gross thermal efficiency, net thermal efficiency, and net fuel conversion efficiency. For more information on the definitions of efficiencies, please see Heywood [22, 51]. As the compression ratio increases, the gross thermal efficiency increases. For each compression ratio, the gross thermal efficiency strictly reduces with increasing PRF number due to the effects of higher intake temperature on charge density. The minimum gross thermal efficiency for all cases is 40% which appears at the highest PRF number case at CR = 8. The maximum is 46% for the lowest PRF number of CR = 15. This figure shows that intake temperature is a key factor in the efficiency of the thermodynamic cycle and in order to obtain higher gross thermal efficiencies, lower intake temperatures should be utilized. A similar trend appears for the net thermal efficiency in Figure 17, which also increases with higher compression ratios and decreases with higher intake temperatures. The difference between the gross and net thermal efficiencies is caused by the open cycle effects and the pumping losses. HCCI engines generally have very low pumping losses. In this case, this CFR engine's valve timings are imposing a ~5.5 percentage point efficiency loss. The maximum net thermal efficiency is 41% at CR = 15, PRF90, and the minimum value is 35% at CR = 8, PRF10. Combustion efficiency is not considered when calculating the gross and net thermal efficiency. Therefore, the net fuel conversion efficiency is also shown in Figure 17. The difference between the net fuel conversion efficiency and the net thermal efficiency is the combustion efficiency. The net fuel conversion efficiency is relatively constant within each compression ratio, especially for the lower compression ratios, which shows that the combustion efficiency is higher for the higher intake temperature cases. Additionally, the difference between the net fuel conversion efficiency and the net thermal efficiency is slightly smaller at higher compression ratios (and higher peak temperatures). For instance, at PRF0 the difference between the net thermal and net fuel conversion efficiencies is 4.0 percentage points, while at PRF96, this difference is 2.9 percentage points.

These results show that the increasing compression ratio and its effect on the thermodynamic cycle is able to outweigh the increased heat transfer losses at higher compression ratio and the slight decrease in the ratio of specific heats. However, these competing factors cause the increase in efficiency with compression ratio to be smaller than the ideal cycle would suggest. As a result, the increase in efficiency with compression ratio is subtle, especially for the mid-range compression ratios. From CR = 8 to 9 to 10, there is a noticeable increase in efficiency. However, CR = 10, 11, 12, 13, and 14 all have very similar efficiencies, with only subtle differences between them. This shows that the increasing expansion work associated with the higher compression ratios is counterbalanced by the higher heat transfer losses and the slightly lower ratio of specific heats. Additionally, these results have shown that lower compression ratios have their advantages (NOx emissions and lower maximum pressure rise rates), which should also be considered.

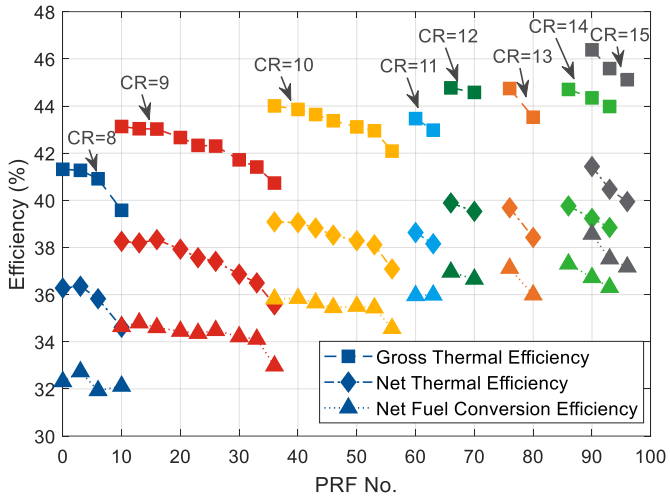

Figure 17. Gross thermal efficiency, net thermal efficiency, and net fuel conversion efficiency at different compression ratios versus PRF number for all of the data collected

Combustion Efficiency and Emissions

Figure 18 shows the combustion efficiency calculated from the measured exhaust gases for all of the data collected. For each specific compression ratio, the combustion efficiency increases with PRF number, which is due to the increasing intake temperature which helps oxide the fuel. This appears most significantly for the lower

compression ratio cases, where the combustion efficiency is generally lower. The combustion efficiency is higher for the higher compression ratio cases because the peak bulk gas temperature is higher.

To illustrate this trend, the combustion efficiency for all of the data collected is plotted against the peak bulk gas temperature in Figure 19. The color bar on the right side of the figure represents the different PRF numbers. In this plot, the combustion efficiency increases with peak bulk gas temperature rapidly until approximately 1500 K. The minimum combustion efficiency appears at 1346 K with value 89% and the highest combustion efficiency is 94% at 1526 K. Above, approximately 1500 K, a coherent trend is hard to distinguish – however, the slope is considerably shallower above 1500 K. Since combustion efficiency is affected by the reaction process that converts CO to CO_2, an investigation of CO is expounded in Figure 20. Emission index (EI) is the ratio of the mass of a particular species of emissions to the mass of fuel injected and it is a way of representing the emissions in a normalized manner. The equation of EI is shown below [52, 53]:

$$EI_i = \frac{\chi_i}{\sum \chi_j} \times \frac{xMW_i}{MW_f} \quad (4)$$

where EI_i is the emission index of species i, χ_i is the mole fraction of species i, χ_j is the mole fractions of any species j, x is the number of moles of carbon in a mole of fuel, MW_i is the molecular weight of species i, and MW_f is the molecular weight of fuel.

A very clear trend can be seen in the CO emissions in Figure 20. As the peak temperature increases, the CO emissions decrease. In Figure 19, the maximum EICO emissions is 265.8 g/kg of fuel at a peak bulk gas temperature of 1346 K, and the minimum EICO emissions is 80.6 g/kg at 1584 K. Around approximately 1500 K, the slope of the EICO emissions with peak temperature changes. Figure 19 and Figure 20 illustrate the importance of peak temperature in the combustion efficiency in HCCI because as the peak temperature decreases the oxidation of CO to CO_2 greatly decreases, with a threshold approximately around 1500 K. This result generally agrees well with Sjoberg and Dec who found the temperature threshold for sufficient OH concentrations to oxidize the CO was approximately 1500 K [31]. Meanwhile, the threshold for thermal NOx production is around 1900 K. Therefore, these results suggest that HCCI combustion should target peak temperatures above 1500 K and below 1900 K, which is a relatively narrow range of peak temperature. It is also important to note that the parent fuel chemistry did not affect the correlation of CO versus peak temperature.

The EI of total hydrocarbon emissions is shown in Figure 21. Unburned hydrocarbon emissions are generated from the cooler areas existing in the chamber near the walls or in the crevices between the piston and the wall. It is important to note that the top-land crevice on this CFR engine is much larger than modern production engines, therefore resulting in elevated unburned hydrocarbon emissions. Unlike CO, the unburned hydrocarbon emissions show a counterintuitive trend with peak temperature and the opposite trend of the EICO emissions. Unburned hydrocarbon emissions in HCCI combustion are generated from regions of the cylinder with lower temperatures, either near the wall or in the crevices. Figure 21 shows that as the peak temperature increases, the EIHC emissions increase. This result is most likely attributed to the increasing PRF number. The color bar shows that the highest PRF number blends produce the highest EIHC emissions, whereas the lower PRF number blends produce the lowest EIHC. Additionally, the amount of mass stored in the crevices, which contribute to the unburned hydrocarbon emissions, increases with the higher compression ratios associated with the higher PRF number fuels. This crevice storage effect and its trend with compression ratio also contributes to the counterintuitive trend in Figure 21. These findings show that CO emissions are most directly related to the peak temperature to drive the CO oxidation, but are not sensitive to the parent fuel; whereas the HC emissions are directly related to the parent fuels autoignition chemistry to start the reactions, and peak temperature is less of a factor in the HC emissions compared to the CO emissions.

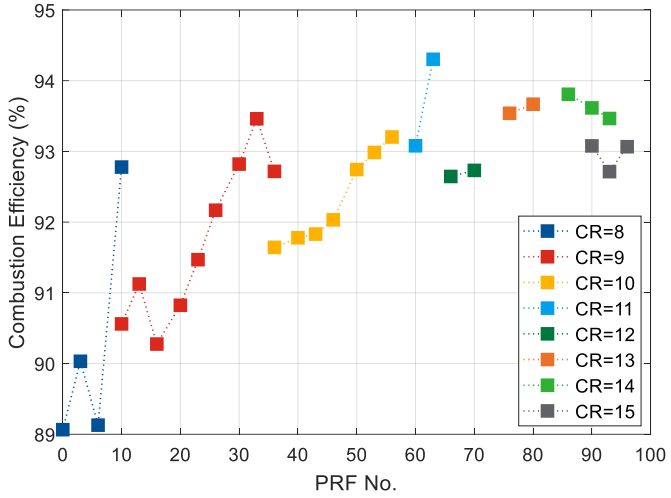

Figure 18. Combustion efficiency at different compression ratios versus PRF number for all of the data collected

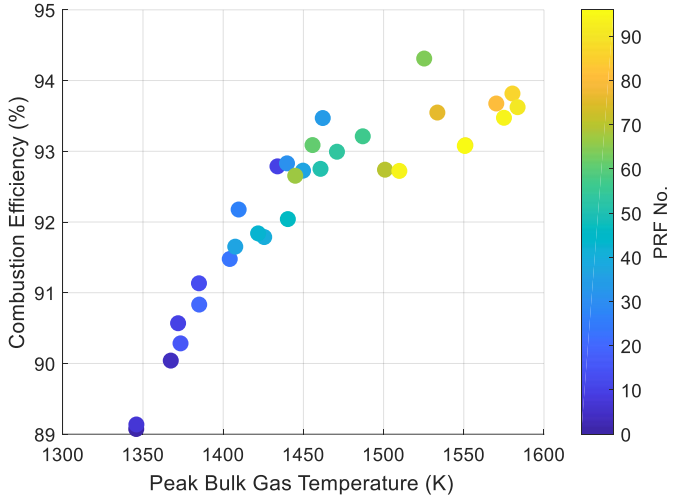

Figure 19. Combustion efficiency vs peak in-cylinder temperature for all of the data collected

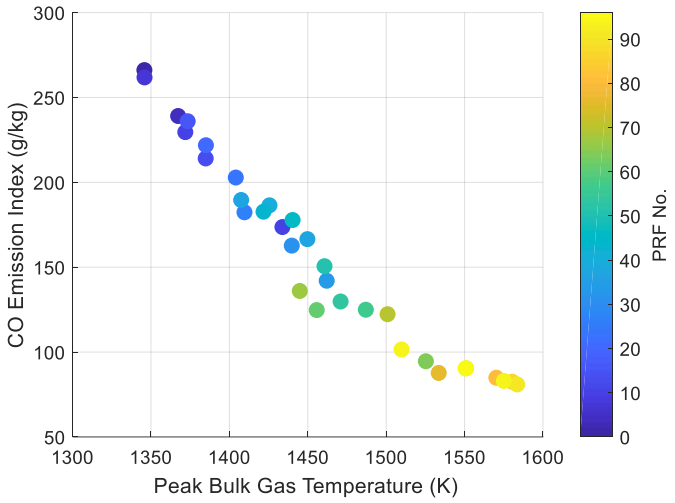

Figure 20. EICO emissions vs peak in-cylinder temperature for all of the data collected

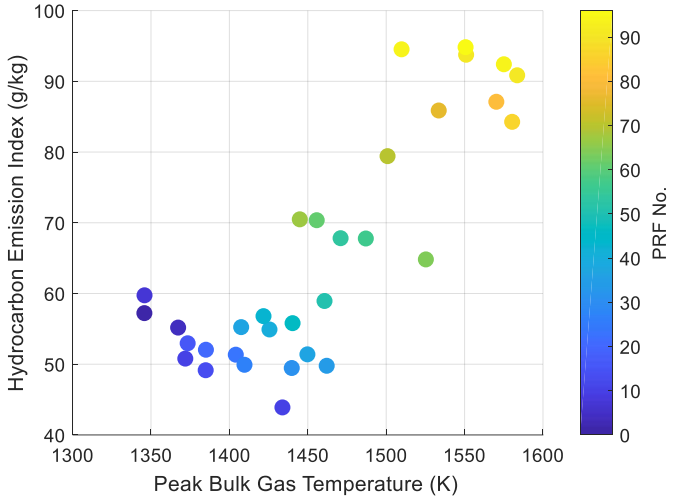

Figure 21. Unburned hydrocarbon emissions vs peak in-cylinder temperature for all of the data collected

Conclusions

This paper demonstrates the effects of a wide range of compression ratios, intake temperatures, and PRF number fuels on the thermodynamics and the combustion process in HCCI combustion. Twenty-eight PRF mixtures were tested in a CFR engine in HCCI with a constant equivalence ratio and combustion phasing. The experimental results were further analyzed using GT-Power to better understand the thermodynamics. The following conclusions can be drawn from the results:

1. Intake temperature and/or compression ratio can be used to adjust the autoignition timing of PRF fuels over a wide range of autoignition properties where higher temperatures and/or compression ratios are needed to autoignite higher PRF number mixtures in HCCI combustion.
2. The peak pressure and bulk gas temperature increase with compression ratio, which results in higher heat transfer coefficients and higher heat loss rates during combustion. However, the expansion to lower temperatures for the higher compression ratios results in lower heat transfer rates after combustion and throughout the expansion process, which partially counterbalances the increasing heat transfer with compression ratio. The cumulative heat loss increases with compression ratio.
3. The maximum pressure rise rate shows a very strong trend with compression ratio, which could potentially allow the increase of the maximum load in HCCI by lowering the compression ratio.
4. Additionally, fuels with significant two-stage ignition can be used to decrease the peak heat release and pressure rise rates in HCCI, potentially leading to higher maximum loads.
5. IMEPg decreases with intake temperature due to the lower densities, regardless of compression ratio.
6. The gross thermal efficiency, net thermal efficiency, and net fuel conversion efficiency increase with compression ratio and decrease with increasing intake temperature. However, the increase in efficiency with compression ratio is subtle above a compression ratio of 10 because the increasing heat transfer losses and decreasing ratio of specific heats partially offset the increasing expansion work with higher compression ratios.
7. The combustion efficiency increases with peak in-cylinder temperature with a steeper slope below 1500 K due to the oxidation of CO. This trend is independent of the parent fuel.
8. Unburned hydrocarbon emissions strongly depend on the parent fuel's autoignition chemistry, with less dependence on the peak bulk temperature, in contrast to the CO emissions.
9. The higher peak pressures associated with higher compression ratios causes an increase in unburned hydrocarbon emissions due to the increase in the crevice storage effect.

Acknowledgments

The authors wish to gratefully acknowledge the financial support of the Department of Energy under award number DE-EE0007216.

References

1. Najt, Paul M, and David E Foster. "Compression-Ignited Homogeneous Charge Combustion." SAE Technical Paper, 1983.
2. Noguchi, Masaaki, Yukiyasu Tanaka, Taro Tanaka, and Yukihisa Takeuchi. "A Study on Gasoline Engine Combustion by Observation of Intermediate Reactive Products During Combustion." SAE International, 1979.
3. Onishi, Shigeru, Souk Hong Jo, Katsuji Shoda, Pan Do Jo, and Satoshi Kato. "Active Thermo-Atmosphere Combustion (Atac)-a New Combustion Process for Internal Combustion Engines." SAE Technical Paper, 1979.
4. Aoyama, Taro, Yoshiaki Hattori, Jun'ichi Mizuta, and Yasuo Sato. "An Experimental Study on Premixed-Charge Compression Ignition Gasoline Engine." SAE International, 1996.
5. Olsson, Jan-Ola, Per Tunestål, Jonas Ulfvik, and Bengt Johansson. "The Effect of Cooled Egr on Emissions and Performance of a Turbocharged Hcci Engine." SAE International, 2003.
6. Suzuki, Hisakazu, Noriyuki Koike, Hajime Ishii, and Matuo Odaka. "Exhaust Purification of Diesel Engines by Homogeneous Charge with Compression Ignition Part 1:

Experimental Investigation of Combustion and Exhaust Emission Behavior under Pre-Mixed Homogeneous Charge Compression Ignition Method." SAE International, 1997.
7. Epping, Kathi, Salvador Aceves, Richard Bechtold, and John E. Dec. "The Potential of Hcci Combustion for High Efficiency and Low Emissions." SAE International, 2002.
8. Nakagome, Keiichi, Naoki Shimazaki, Keiichi Niimura, and Shinji Kobayashi. "Combustion and Emission Characteristics of Premixed Lean Diesel Combustion Engine." SAE technical paper, 1997.
9. Jiménez-Espadafor, Francisco J, Miguel Torres, José A Velez, Elisa Carvajal, and José A Becerra. "Experimental Analysis of Low Temperature Combustion Mode with Diesel and Biodiesel Fuels: A Method for Reducing Nox and Soot Emissions." *Fuel Processing Technology* 103 (2012): 57-63.
10. Lapuerta, Magin, Octavio Armas, and Jose Rodriguez-Fernandez. "Effect of Biodiesel Fuels on Diesel Engine Emissions." *Progress in energy and combustion science* 34, no. 2 (2008): 198-223.
11. McCarthy, Peter, MG Rasul, and Shadia Moazzem. "Analysis and Comparison of Performance and Emissions of an Internal Combustion Engine Fuelled with Petroleum Diesel and Different Bio-Diesels." *Fuel* 90, no. 6 (2011): 2147-57.
12. Pramanik, K. "Properties and Use of Jatropha Curcas Oil and Diesel Fuel Blends in Compression Ignition Engine." *Renewable energy* 28, no. 2 (2003): 239-48.
13. Agarwal, Deepak, and Avinash Kumar Agarwal. "Performance and Emissions Characteristics of Jatropha Oil (Preheated and Blends) in a Direct Injection Compression Ignition Engine." *Applied thermal engineering* 27, no. 13 (2007): 2314-23.
14. Chauhan, Bhupendra Singh, Naveen Kumar, Yong Du Jun, and Kum Bae Lee. "Performance and Emission Study of Preheated Jatropha Oil on Medium Capacity Diesel Engine." *Energy* 35, no. 6 (2010): 2484-92.
15. Kimura, Shuji, Osamu Aoki, Hiroshi Ogawa, Shigeo Muranaka, and Yoshiteru Enomoto. "New Combustion Concept for Ultra-Clean and High-Efficiency Small Di Diesel Engines." SAE Technical Paper, 1999.
16. Ryan, Thomas W, and Timothy J Callahan. "Homogeneous Charge Compression Ignition of Diesel Fuel." SAE Technical Paper, 1996.
17. Zhao, Fuquan, Thomas W Asmus, Dennis N Assanis, John E Dec, James A Eng, and Paul M Najt. "Homogeneous Charge Compression Ignition (Hcci) Engines: Key Research and Development Issues Pt-94." *Progress in Technology* 94 (2003).
18. Zhao, Fuquan, Thomas N Asmus, Dennis N Assanis, John E Dec, James A Eng, and Paul M Najt. "Homogeneous Charge Compression Ignition (Hcci) Engines." SAE Technical Paper, 2003.
19. Gray, Allen W Bill, and Thomas W Ryan. "Homogeneous Charge Compression Ignition (Hcci) of Diesel Fuel." SAE Technical Paper, 1997.
20. Lawler, Benjamin, Joshua Lacey, Nicolas Dronniou, Jeremie Dernotte, John E. Dec, Orgun Guralp, Paul Najt, and Zoran Filipi. "Refinement and Validation of the Thermal Stratification Analysis: A Post-Processing Methodology for Determining Temperature Distributions in an Experimental Hcci Engine." SAE International, 2014.
21. Mamalis, Sotirios, Aristotelis Babajimopoulos, Orgun Guralp, and Paul Najt. "Optimal Use of Boosting Configurations and Valve Strategies for High Load Hcci - a Modeling Study." SAE International, 2012.
22. Heywood, John B. *Internal Combustion Engine Fundamentals*. Vol. 930: Mcgraw-hill New York, 1988.
23. Lawler, Benjamin, Elliott Ortiz-Soto, Rohit Gupta, Huei Peng, and Zoran Filipi. "Hybrid Electric Vehicle Powertrain and Control Strategy Optimization to Maximize the Synergy with a Gasoline Hcci Engine." *SAE International Journal of Engines* 4, no. 2011-01-0888 (2011): 1115-26.
24. Lawler, Benjamin, Derek Splitter, James Szybist, and Brian Kaul. "Thermally Stratified Compression Ignition: A New Advanced Low Temperature Combustion Mode with Load Flexibility." *Applied Energy* 189 (2017): 122-32.
25. Mamalis, Sotirios, Aristotelis Babajimopoulos, Dennis Assanis, and Claus Borgnakke. "A Modeling Framework for Second Law Analysis of Low-Temperature Combustion Engines." *International Journal of Engine Research* 15, no. 6 (2014): 641-53.
26. Mamalis, Sotirios, Aristotelis Babajimopoulos, Orgun Guralp, Paul M Najt, and Dennis N Assanis. "The Interaction between Compression Ratio, Boosting and Variable Valve Actuation for High Load Homogeneous Charge Compression Ignition: A Modeling Study." *International Journal of Engine Research* 15, no. 4 (2014): 460-70.
27. Lawler, Benjamin J, and Zoran S Filipi. "Integration of a Dual-Mode Si-Hcci Engine into Various Vehicle Architectures." *Journal of Engineering for Gas Turbines and Power* 135, no. 5 (2013): 052802.
28. Mamalis, Sotirios, Vishnu Nair, Peter Andruskiewicz, Dennis N. Assanis, Aristotelis Babajimopoulos, Nicole Wermuth, and Paul Najt. "Comparison of Different Boosting Strategies for Homogeneous Charge Compression Ignition Engines - a Modeling Study." *SAE International Journal of Engines* 3, no. 1 (2010): 296-308.
29. Tanaka, Shigeyuki, Ferran Ayala, and James C Keck. "A Reduced Chemical Kinetic Model for Hcci Combustion of Primary Reference Fuels in a Rapid Compression Machine." *Combustion and flame* 133, no. 4 (2003): 467-81.
30. Soyhan, Hakan Serhad, Fabian Mauss, and Cem Sorusbay. "Chemical Kinetic Modeling of Combustion in Internal Combustion Engines Using Reduced Chemistry." *Combustion Science and Technology* 174, no. 11-12 (2002): 73-91.
31. Sjöberg, Magnus, and John E Dec. "An Investigation into Lowest Acceptable Combustion Temperatures for Hydrocarbon Fuels in Hcci Engines." *Proceedings of the Combustion Institute* 30, no. 2 (2005): 2719-26.
32. Mamalis, Sotirios, and Aristotelis Babajimopoulos. "Model-Based Estimation of Turbocharger Requirements for Boosting an Hcci Engine." *Ann Arbor* 1001 (2010): 48109.
33. Mamalis, S, and DN Assanis. "Second-Law Analysis of Boosted Hcci Engines: Modeling Study." *Journal of Energy Engineering* 141, no. 2 (2014): C4014014.
34. Lawler, Benjamin, Sotirios Mamalis, Satyum Joshi, Joshua Lacey, Orgun Guralp, Paul Najt, and Zoran Filipi. "Understanding the Effect of Operating Conditions on Thermal Stratification and Heat Release in a Homogeneous Charge Compression Ignition Engine." *Applied Thermal Engineering* 112 (2017): 392-402.
35. Lawler, Benjamin, Satyum Joshi, Joshua Lacey, Orgun Guralp, Paul Najt, and Zoran Filipi. "Understanding the Effect of Wall Conditions and Engine Geometry on Thermal Stratification and Hcci Combustion." Paper presented at the Proceedings of the ASME 2014 internal combustion engine

division fall technical conference, ICEF2014-5687, Columbus, Indiana, USA, 2014.
36. Ebrahimi, R. "Effect of Specific Heat Ratio on Heat Release Analysis in a Spark Ignition Engine." *Scientia Iranica* 18, no. 6 (2011): 1231-36.
37. Yao, Mingfa, Zhaolei Zheng, and Haifeng Liu. "Progress and Recent Trends in Homogeneous Charge Compression Ignition (Hcci) Engines." *Progress in Energy and Combustion Science* 35, no. 5 (2009): 398-437.
38. Christensen, Magnus, Anders Hultqvist, and Bengt Johansson. "Demonstrating the Multi Fuel Capability of a Homogeneous Charge Compression Ignition Engine with Variable Compression Ratio." SAE International, 1999.
39. Christensen, Magnus, and Bengt Johansson. "Supercharged Homogeneous Charge Compression Ignition (Hcci) with Exhaust Gas Recirculation and Pilot Fuel." SAE Technical Paper, 2000.
40. Hyvönen, Jari, Göran Haraldsson, and Bengt Johansson. "Supercharging Hcci to Extend the Operating Range in a Multi-Cylinder Vcr-Hcci Engine." SAE Technical Paper, 2003.
41. Milovanovic, Nesa, Rui Chen, and JWG Turner. "Influence of the Variable Valve Timing Strategy on the Control of a Homogeneous Charge Compression (Hcci) Engine." (2004).
42. Christensen, Magnus, Bengt Johansson, and Patrik Einewall. "Homogeneous Charge Compression Ignition (Hcci) Using Isooctane, Ethanol and Natural Gas - a Comparison with Spark Ignition Operation." SAE International, 1997.
43. Haraldsson, Göran, Per Tunestål, Bengt Johansson, and Jari Hyvönen. "Hcci Combustion Phasing in a Multi Cylinder Engine Using Variable Compression Ratio." SAE International, 2002.
44. Szybist, James P., and Bruce G. Bunting. "The Effects of Fuel Composition and Compression Ratio on Thermal Efficiency in an Hcci Engine." SAE International, 2007.
45. Aroonsrisopon, Tanet, David E. Foster, Takeshi Morikawa, and Minoru Iida. "Comparison of Hcci Operating Ranges for Combinations of Intake Temperature, Engine Speed and Fuel Composition." SAE International, 2002.
46. Lü, Xing-cai, Wei Chen, Yu-chun Hou, and Zhen Huang. "Study on the Ignition, Combustion and Emissions of Hcci Combustion Engines Fueled with Primary Reference Fuels." SAE Technical Paper, 2005.
47. Yao, Mingfa, Bo Zhang, Zunqing Zheng, Zheng Cheng, and Yuan Xing. "Experimental Study on the Effects of Egr and Octane Number of Prf Fuel on Combustion and Emission Characteristics of Hcci Engines." SAE Technical Paper, 2005.
48. Machrafi, Hatim, Simeon Cavadias, and Philippe Gilbert. "An Experimental and Numerical Analysis of the Hcci Auto-Ignition Process of Primary Reference Fuels, Toluene Reference Fuels and Diesel Fuel in an Engine, Varying the Engine Parameters." *Fuel processing technology* 89, no. 11 (2008): 1007-16.
49. Truedsson, Ida, William Cannella, Bengt Johansson, and Martin Tuner. "Engine Speed Effect on Auto-Ignition Temperature and Low Temperature Reactions in Hcci Combustion for Primary Reference Fuels." SAE Technical Paper, 2014.
50. Hohenberg, Günter F. "Advanced Approaches for Heat Transfer Calculations." SAE Technical Paper, 1979.
51. Christensen, Magnus, and Bengt Johansson. "Homogeneous Charge Compression Ignition with Water Injection." SAE Technical Paper, 1999.
52. Law, Chung K. *Combustion Physics*. Cambridge university press, 2010.
53. Turns, Stephen R. *An Introduction to Combustion*. Vol. 287: McGraw-hill New York, 1996.

Contact Information

Benjamin Lawler – benjamin.lawler@stonybrook.edu

Definitions/Abbreviations

IVO	Intake valve open
IVC	Intake valve close
EVO	Exhaust valve open
EVC	Exhaust valve close
TDC	Top dead center
aTDC	After top dead center
HCCI	Homogeneous charged compression ignition
CR	Compression ratio
IMEPg	Gross indicated mean effective pressure
LTHR	Low temperature heat release
HTHR	High temperature heat release
MPRR	Maximum pressure rise rate
MTRR	Maximum temperature rise rate
CA50	Crank angle location where 50% of heat has released
CAD	Crank angle degree
SI	Spark ignition
CI	Compression ignition
PRF	Primary reference fuel
COV	Coefficient of variation
EI	Emission index